Journal of Materials Chemistry A

ROYAL SOCIETY OF CHEMISTRY

PAPER

View Article Online
View Journal | View Issue

Cite this: J. Mater. Chem. A, 2020, 8, 8462

Compatibilizing hydrophilic and hydrophobic polymers *via* spray coating for desalination†

Junquan Meng,[a] Cher Hon Lau, *[b] Yunlong Xue,[a] Rui Zhang,[a] Bing Cao*[a] and Pei Li *[a]

Received 21st January 2020
Accepted 3rd April 2020

DOI: 10.1039/d0ta00871k

rsc.li/materials-a

The incompatibility between hydrophobic polymers such as polytetrafluoroethylene (PTFE) and hydrophilic polymers such as polyvinyl alcohol (PVA) is typically overcome by reducing the large surface energy difference between these materials *via* complex protocols or using bespoke chemicals. In this study, we deployed the simple technique of spray coating to solve this incompatibility, depositing polyvinyl alcohol (PVA) onto PTFE porous support layers. This was achieved as sub-micron sized PVA solution droplets infiltrated and filled up PTFE inter-fiber pores, forming a tightly bound PVA layer on PTFE fibrous supports. The defect-free thin hydrophilic PVA layer and the porous hydrophobic PTFE substrate of the composites were exploited for desalination in both direct contact membrane distillation (DCMD) and pervaporation (PV) modes. When deployed to separate 3.5 wt% NaCl from water at 75.0 ± 0.9 °C with a permeate side pressure of 100 Pa in PV mode, these thin film composites demonstrated ultra-high water fluxes of 143.4 ± 8.9 kg m^{-2} h^{-1}, outperforming state-of-the-art PV membranes. Moreover, when the membrane was tested in DCMD mode with a cooling stream at 20.6 ± 0.3 °C, a water flux of 64.2 ± 2.9 kg m^{-2} h^{-1} was obtained and was on par with the best DCMD membranes. With excellent organic and ionic fouling resistances, these thin film composites can be potentially deployed to treat polluted brine mixtures, even under harsh operating conditions.

Introduction

Polymer membrane separation is a low-energy alternative to incumbent separation technologies such as distillation and adsorption.[1] As such, membrane technologies are deployed in nearly 70% of desalination plants around the world to extract fresh water from brackish water and seawater.[2] The heart of this technology is the polymer membrane – typically a thin film composite (TFC) comprising thin, dense selective layers deposited on porous supports. As polymers deployed in the selective and support layers of industrial membranes are hydrophobic,[3] these membranes are prone to bio- and organic fouling and will require frequent cleaning cycles for recovering their initial high separation performances *i.e.* down time is incurred.[4–6] Fouling can be reduced by using hydrophilic selective layers,[7,8] but such materials are incompatible with existing hydrophobic porous supports, often resulting in delamination that hinders membrane's long term stability.[9–11]

To overcome the incompatibility between hydrophilic and hydrophobic polymers, it is important to understand the forces involved in the adhesion of a coating layer to substrates. These forces include: (1) chemical bonds; (2) physical attraction due to van der Waals forces, hydrogen bonding and electrostatic attraction; (3) mechanical interlocking due to penetration of adhesives into pores of support layers; and (4) diffusion of adhesives into the bulk phase of supports.[12] Techniques that facilitate these forces for preventing delamination of incompatible polymers include chemical modification,[13–15] irradiation grafting,[16,17] plasma treatment[18,19] and double scratching (or joint extrusion)[20,21] and they introduce chemical bonding or strengthen physical attractions. Though effective, these protocols are complex and materials-specific.

A simple approach to overcome the incompatibility between hydrophilic and hydrophobic polymers is to fill pre-wetted surface pores with a polymer coating to achieve mechanical interlocking (Fig. 1).[12,22] This typically requires an intermediary layer or a gutter layer to compatibilise the large difference in the surface energies between polymers. For example, in our previous work,[23] we deployed polyvinylidene fluoride (PVDF) to overcome the incompatibility between hydrophilic polyvinyl alcohol (PVA) and polytetrafluoroethylene (PTFE), a hydrophobic polymer. The surface energy of PVDF was lower than that of PVA; hence PVDF could partially wet the PTFE porous

[a]College of Materials Science and Engineering, Beijing University of Chemical Technology, Beijing, 100029, China. E-mail: lipei@mail.buct.edu.cn; bcao@mail.buct.edu.cn

[b]School of Engineering, The University of Edinburgh, Robert Stevenson Road, EH3 9BR, UK. E-mail: Cherhon.Lau@ed.ac.uk

† Electronic supplementary information (ESI) available. See DOI: 10.1039/d0ta00871k

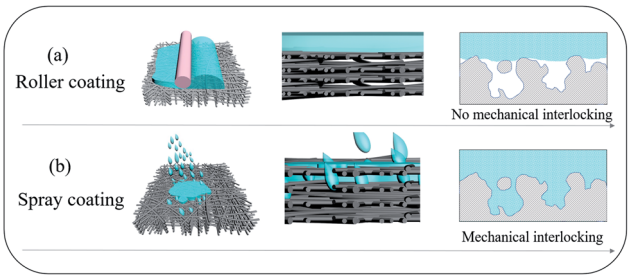

Fig. 1 Schematic diagrams of (a) roller coating, and (b) spray coating to produce thin film polymer composites from incompatible polymers.

substrate to achieve a higher adhesion force. Meanwhile, compared to that of PTFE, the surface energy of PVDF was higher, enabling a stronger physical attraction to the PVA layer. However, this PVDF gutter layer increased resistance to molecular transport, limiting the separation performances.[23] Clearly, a facile and more effective technique is required to overcome the incompatibility between PVA and PTFE.

We report here a highly efficient and simple technique to overcome PVA–PTFE incompatibility. By spray-coating aqueous PVA solutions on to commercial PTFE nanofibrous porous supports produced from biaxial stretching, the atomized PVA/water droplets could penetrate into the surface pores and fill the gaps between sub-layer fibres of the PTFE supports (Fig. 1). A strong mechanical interlocking structure was formed at the interface between PTFE fibers and the PVA coating layer. This was key to resolving the delamination problem of PVA layers from PTFE supports in these thin film composites. The lack of a gutter layer between the hydrophilic selective layer and hydrophobic porous support minimized resistance to water transport, imparting excellent desalination performances to our PVA/PTFE thin film composites in various modes – pervaporation (PV) and direct contact membrane distillation (DCMD). Even in the presence of organic foulants, the deployment of our PVA/PTFE composites in PV and DCMD modes outperformed state-of-the-art and commercial desalination membranes, respectively.

Experimental

Materials

PTFE microfiltration membranes (average pore size – 317.6 nm) were purchased from the Beijing Shenghe Integrity Membrane Science and Technology Development Center (China). PVDF (purity ≥ 99.5%) was purchased from Sigma Aldrich, while polyvinylpyrrolidone (PVP K-30, purity ≥ 95.0%) was obtained from Gobekie Co., Ltd. LiCl (purity ≥ 95%) and NMP (purity ≥ 99.0%) was purchased from the Tianjin Fuchen Chemical Reagent Factory (China). Poly(vinyl alcohol) (PVA124, hydrolysis degree: 99.4%), sodium chloride (NaCl, purity ≥ 99.5%), and Tween 20 were acquired from Sinopharm Chemical Reagent Co., Ltd (China). An aqueous solution comprising 50 wt% 4-sulfophthalic acid (SPTA) was obtained from Tokyo Chemical Industry Co., Ltd and deionised water was obtained from a Millipore ultrapure water system.

Membrane fabrication

Roller-coating. PVA/PVDF/PTFE three-layer composite membranes were prepared *via* the non-solvent induced phase inversion method (NIPS) based on a previously reported method[23] and used as control samples in this work. Briefly, a dope solution containing PVDF/PVP/LiCl/NMP (weight ratio – 20/3/3/100) was deposited on to 50 μm thick PTFE supports by knife-casting. These composites were immersed in a 25 °C water bath to form PVDF/PTFE ultrafiltration membranes. Residual NMP and additives were removed from these membranes *via* water washes. Water-wet PVDF/PTFE membranes were dried in air for 24 h at room temperature. An aqueous solution containing 2 wt% PVA/SPTA (5/4 w/w) was roller-coated on to the PVDF/PTFE membranes (Fig. 1a). This formulation was based on our previous work where we reported optimised crosslinking of PVA selective layers using SPTA for PV desalination.[24,25] The volume of the coating solution was controlled at 32 μL cm^{-2} using a micro-pipette. The PVA/PVDF/PTFE membranes were dried in air for 6 h at room temperature and heated to 100 °C for 2 h to crosslink the PVA layer with SPTA *via* esterification. PVA crosslinking is required to prevent dissolution in water.[23] This protocol was also deployed to fabricate PVA/PTFE thin-film composite membranes (RC-PVA/PTFE) here.

Spray-coating. An aqueous solution containing 0.75 wt% PVA/SPTA (5/4 w/w) was spray-coated on to a PTFE membrane. The spray system (USTAR, China) comprised an air brush (S-120, nozzle diameter: 0.2 mm) and a mini air compressor (UA-601G). During spraying, the nozzle-surface distance and air pressure were maintained at 10 cm and 2.5 bar, respectively. Each spray lasted for 2–4 s, depositing 42 μL cm^{-2} PVA/SPTA solution on the PTFE membranes and dried by using an air blower prior to another coating. We tailored PVA layer thicknesses by varying the number of sprays (1–4), producing PVA selective layers of 1–5.2 μm. Finally, the PVA/PTFE membranes were heated at 100 °C for 2 h to crosslink PVA. Table 1 summarises the nomenclature of all the membranes studied here, PVA thicknesses and the number of sprays required.

Membrane characterisation

Physicochemical properties. A scanning electron microscope (SEM) (HITACHI S-7800 Japan) was used to characterise the cross-section, surface and interface morphologies of the membranes studied here. Cross-sectional micrographs were obtained from the composites fractured in liquid nitrogen. The

Table 1 The nomenclature of all the membranes studied here, PVA thicknesses and the number of sprays required

Membrane type	Technique	PVA thickness	No. of coats
PVA/PVDF/PTFE	NIPS	2.4 μm	N.A.
RC-PVA/PTFE	Roller coating	3.2 μm	1
SC-1-PVA/PTFE	Spray coating	1.0 μm	1
SC-2.6-PVA/PTFE		2.6 μm	2
SC-3.5-PVA/PTFE		3.5 μm	3
SC-5.2-PVA/PTFE		5.2 μm	4

thicknesses of dense PVA selective layers were determined from cross-sectional SEM images using Nano Measurer software. The adhesive strength between PVA dense selective layers and PTFE membranes was measured using a dynamic mechanical analyzer (DMA) (Q800, TA, USA) (Fig. S1†). The front and rear surfaces of the composite membrane were affixed between two glass plates using adhesive tape, clamped by using a DMA fixture. The samples were stretched in the control force mode at a rate of 0.2 N min^{-1} until they were torn apart. The highest stress was recorded as the adhesive strength. After the test, fractured surfaces of these composite membranes were characterised using SEM.

Determination of desalination properties. The desalination performances of the pristine PTFE membrane and all the composites were determined using DCMD equipment, where the membrane permeate side was in direct contact with a cooling stream as shown in Fig. 2a. The separation performances of defect-free composite membranes including SC-2.6-PVA/PTFE, SC-3.5-PVA/PTFE and SC-5.2-PVA/PTFE were also characterised by vacuuming the membrane permeate side at 100 Pa (PV mode) using an equipment set-up shown in Fig. 2b. Temperatures of feed solutions comprising 3.5, 5, 10, 20 and 25 wt% NaCl used in these experiments were maintained at 43.4 ± 0.3 to 75.0 ± 0.9 °C.

Direct contact membrane distillation. The DCMD apparatus set-up reported in our previous work[23] was used here. Briefly, 2 L of a hot feed solution (3.5 wt% NaCl in DI water) and 600 mL DI water (20.6 ± 0.3 °C) were circulated on the feed and permeate sides, respectively, at a velocity of 0.14 m s^{-1} controlled by using two peristaltic pumps (WT600S, frei fluid technology co. LTD, China). The effective membrane area was 22.5 cm^2. Weight increment on the permeate side was monitored using an electronic balance and was only recorded after 0.5 h of stabilisation while the conductivity of the cooling water system was measured for at least 20 min. Membrane flux was calculated using eqn (1):

$$J_w = \frac{\Delta m}{A_1 T_1} \quad (1)$$

where J_w is the permeate flux (kg m^{-2} h^{-1}); Δm (kg) is the weight gain over time; and T_1 is the operation period (h). Salt rejection was calculated using eqn (2)

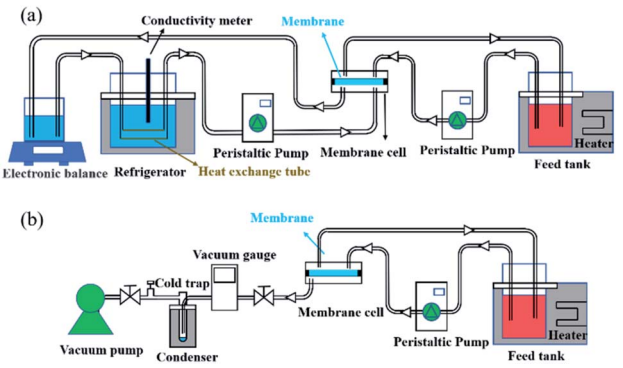

Fig. 2 Schematic diagrams of the (a) DCMD system and (b) PV system.

$$R = \left(1 - \frac{C_p}{C_f}\right) \times 100\% \quad (2)$$

where R is the NaCl rejection (%), and C_f is the NaCl concentration in feed. C_p was estimated using eqn (3).

$$C_p = \frac{\sigma}{1.68} \times \frac{m_1}{m_1 - m_0} \quad (3)$$

where σ is the conductivity of cooling water; and m_0 and m_1 are the masses of cooling water before and after the test. The constant 1.68 was obtained from the fitting curve of conductivity *versus* salt concentration (Fig. S2†). To preserve a stable salt concentration, the feed solution was maintained at 2 L throughout the experiment. In this study, the biggest weight loss of the feed solution was 170 g in 1 h. This corresponded to an increment in NaCl concentration from 3.5 to 3.8 wt%. The conductivity of cooling water was always lower than 20 μS, which was similar to that of DI water. Therefore, a constant driving force could be assumed during the entire duration of the desalination experiments.

Pervaporation (PV). A bespoke PV setup[26] was adopted to test the desalination properties in PV mode. Under vacuum, water vapor was condensed in a liquid nitrogen trap and weighed to calculate water flux using eqn (1). To estimate the salt rejection, DI water of the same mass as condensed water was used to wash the back of the membrane to dissolve any precipitated salt. The salt concentrations of feed and permeate solutions were measured with a conductivity meter and used to calculate salt rejection using eqn (2).

Membrane fouling. To investigate the fouling resistances of the membranes studied here, Tween 20 (an organic oil contaminant) was added to a 3.5 wt% NaCl feed solution at a concentration of 10 mg L^{-1}. The feed and cooling water temperatures were maintained at 75 ± 0.9 and 20.6 ± 0.3 °C, respectively. The on-line water flux was recorded using a computer system, while the solution conductivities were manually measured and recorded. The feed solution was topped up every hour to maintain a constant salt concentration.

Results and discussion

Polymer compatibility

The low surface energy of PTFE resulted in its incompatibility with other materials.[27–30] This was also evident here as roller-coated PVA layers delaminated from the PTFE fibrous supports (Fig. 3a). Since the PVA solution could not wet and permeate into the inter-fibre pores of the PTFE support, the poor physical attractions between the PVA layer and the PTFE support were too weak to enable firm adhesion of PVA layers. Meanwhile, spray-coated PVA layers adhered to the support layer, forming a tightly bound interlayer structure (Fig. 3b). The difference in structural stability was attributed to the ability to infiltrate inter-PTFE fiber pores by sub-micron sized PVA droplets. From Fig. S4,† we observed that PVA droplets first wrapped around PTFE fibers after one second of spray coating, and then formed firmly affixed 350 nm wide PVA

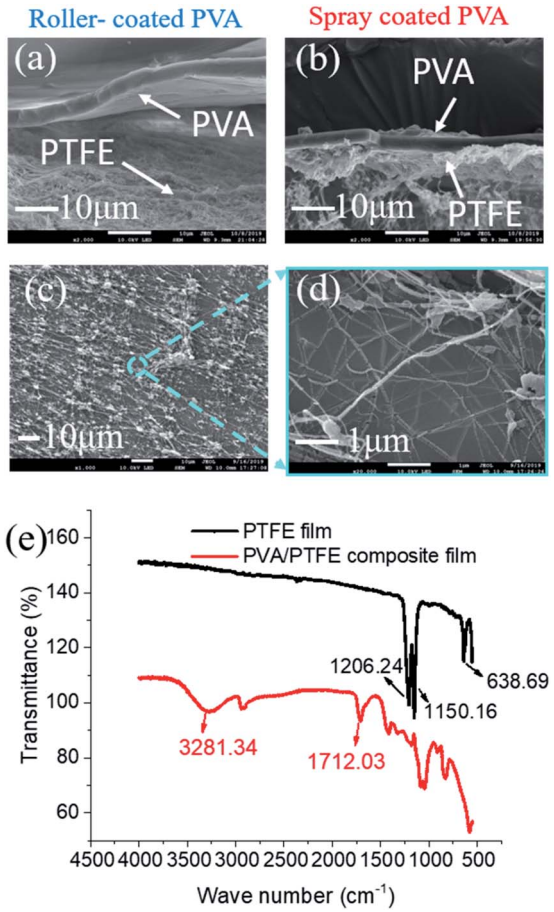

Fig. 3 SEM micrographs of (a) roller coated and (b) spray coated PVA/PTFE composites where delamination of PVA is prevalent in the composites produced from roller coating. (c and d) The bottom surface of PVA selective layers was intertwined with PTFE fibers, indicating excellent compatibility between these materials. (e) The presence of spray coated PVA on PTFE supports was validated with FTIR analysis.

islands on the PTFE fibers after 3 seconds. To explain the observation, we measured the surface tension of the PVA solutions (Fig. S3†), which decreased with the increment in PVA concentration. We also monitored a very fast evaporation process of atomized PVA droplets sprayed on a glass board (video in the ESI†). We hypothesize that the rapid decrements in the surface energy and sizes of the PVA droplets enable them to wet and flow into the pores of the PTFE substrate. After the droplets dried, the PTFE fibers were covered with a thin PVA film and their surfaces became hydrophilic. As more PVA was deposited on to the PVA islands, a dense PVA layer was formed. The improved compatibility between PVA and PTFE was evidenced by a significant amount of PTFE fibers within the PVA matrix, indicating good adhesion (Fig. 3c and d). The presence of PVA spray coated on to the PTFE fibrous support was validated with FTIR analyses (Fig. 3e). The structure (surface and cross-sectional morphology, and thickness of PVA) of the SC-PVA/PTFE composite membranes with different amounts of PVA is shown in Fig. S5 and Table S1.†

Polymer adhesion

As shown in Fig. 4f, the adhesive strength between roller coated PVA layers and PTFE fibrous supports was 0.02 MPa. This was the lowest amongst all the samples studied here and is typical of delaminated layer structures (Fig. 4a1–a3).[20,31–33] The low surface energy of PTFE and the absence of the mechanical interlocking structure between PVA and PTFE resulted in the low adhesive strength between these two topologically different layers.[34] The adhesive strengths of PVDF/PTFE and PVA/PVDF/PTFE composites were similar and 4.5 fold higher than that of PVA/PTFE. Even with an intermediate PVDF layer, delamination remained prevalent, but at the PVDF–PTFE interface (Fig. 4b and c). Clearly, roller coating is not effective for overcoming the drastic differences in the surface energy between PTFE and other polymers studied here. Similar to PVA, PVDF did not infiltrate inter-PTFE fiber pores. Spray coated PVA/PTFE composites demonstrated the highest adhesive strength of 0.15 MPa, which was equivalent to the tearing strength of pristine PTFE fibrous supports as tearing occurred within the PTFE structure (Fig. 4d and e). Clearly, the significantly improved polymer adhesion benefits from the mechanical interlocking structure caused by spray coating.

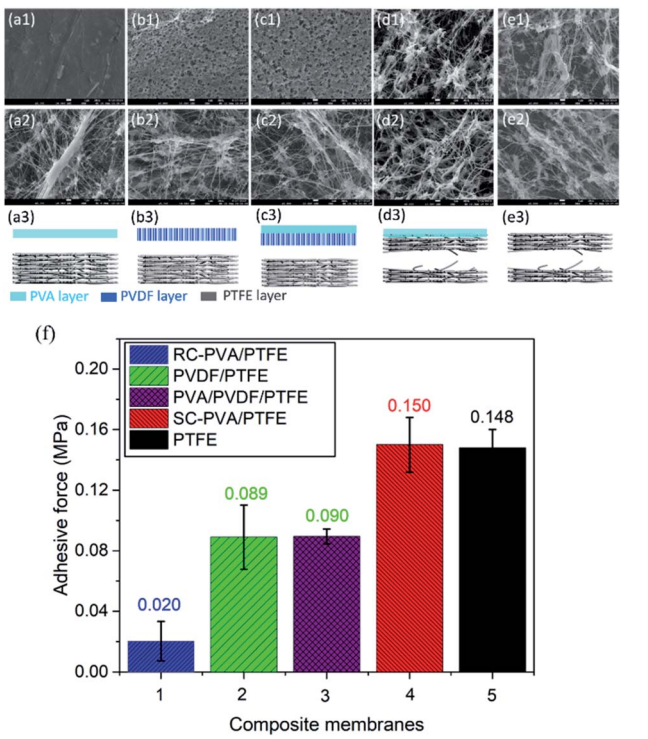

Fig. 4 SEM images of the bottom surface from the top layer and the upper surface of the support layer, and a schematic diagram showing the tearing locations of the RC-PVA/PTFE (a1–a3), PVDF/PTFE (b1–b3), PVA/PVDF/PTFE (c1–c3), SC-PVA/PTFE (d1–d3) and PTFE (e1–e3) membranes. (f) The adhesion strength between PVA dense selective layers and PTFE supports in the composites produced from roller coating and spray coating.

Desalination properties

Desalination properties were assessed using an aqueous solution comprising 3.5 wt% NaCl as feed. All the composite membranes were first tested in DCMD mode and their desalination properties were compared with those of the pristine PTFE membrane. The PVA layers of roller coated composites (RC-PVA/PTFE) were partially delaminated from the PTFE substrate just after 1 h of desalination (Fig. S6†), indicating poor structural integrity and weak adhesion forces between PVA and PTFE. Therefore, desalination performances of RC-PVA/PTFE composites were not assessed. Desalination properties of other membranes were further determined in PV mode except for the PTFE and SC-1-PVA/PTFE composites. This was ascribed to the penetration of the feed solution into the pores of the PTFE support or surface defects of SC-1-PVA/PTFE composites under vacuum.

The water fluxes of these membranes in DCMD modes at feed temperatures of 43.4 ± 0.3 to 75.0 ± 0.9 °C monotonically decreased with thicker PVA layers (Fig. 5a), corresponding to increased water transport resistance in thicker selective layers.[35–39] The presence of an intermediate PVDF layer in roller coated PVA/PVDF/PTFE composites also impacted on water transport, reducing water flux by 42%, from 143.4 ± 8.9 kg m^{-2} h^{-1} to 83.4 ± 6.5 kg m^{-2} h^{-1} (reported in our previous study[23]). Amongst spray-coated defect-free PVA/PTFE thin film composites, SC-2.6-PVA/PTFE membranes demonstrated the highest water flux of 112.1 kg m^{-2} h^{-1} at a feed temperature of 67 °C (Fig. 5b) in PV mode, surpassing the state-of-the-art MXene/PAN composite membrane (85.4 kg m^{-2} h^{-1}, 65 °C (ref. 40)) and PVA/PVDF/PTFE composite membrane (83.4 kg m^{-2} h^{-1}, 70 °C (ref. 23)). The significantly higher water flux of the SC-2.6-PVA/PTFE membrane was attributed to the lower resistance of the PTFE substrate than the PVDF/PTFE support.

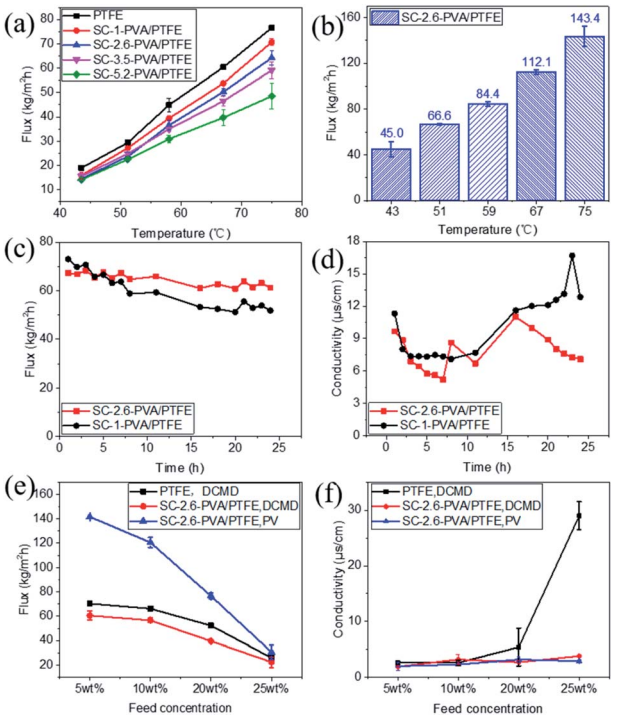

Fig. 5 Desalination properties. (a) Water fluxes in DCMD mode at feed temperatures ranging from 43.4 ± 0.3 to 75.0 ± 0.9 °C; (b) water fluxes in PV mode at a feed temperature of 70 °C; and (c) the desalination properties of the SC-1-PVA/PTFE and SC-2.6-PVA/PTFE composite membranes in DCMD mode over time (feed: 3.5 wt% NaCl solution with 10 mg L^{-1} Tween 20). (d) The conductivity of the cooling water of the SC-1-PVA/PTFE and SC-2.6-PVA/PTFE composite membranes in DCMD mode over time (feed: 3.5 wt% NaCl solution with 10 mg L^{-1} Tween 20); (e) the desalination performances of the PTFE, SC-2.6-PVA/PTFE membranes in DCMD or PV modes using feed solutions containing 5 to 25 wt% NaCl at a temperature of 75.0 ± 0.9 °C; and (f) the conductivity of the permeate solution of PTFE, and SC-2.6-PVA/PTFE membranes using feed solutions containing 5 to 25 wt% NaCl at a temperature of 75.0 ± 0.9 °C.

The presence of defect-free hydrophilic PVA dense selective layers enhanced PTFE resistance towards organic fouling. Tween 20, a widely applied non-ionic surfactant,[41–44] was added to the 3.5 wt% NaCl feed solution to evaluate the anti-fouling properties of spray-coated PVA/PTFE membranes in DCMD mode. Our previous study showed that pores of the hydrophobic PTFE membrane were wetted by the feed solution within 8 h *i.e.* fouling resistance lasted only for 8 hours.[23] In contrast, as shown in Fig. 5c and d, the conductivities of permeate solutions from spray coated PVA/PTFE composites remained stable at 10–15 μs cm^{-1}, even after 16 hours of characterisation, demonstrating that the PTFE substrates were not wetted by the feed solution. The water flux of the SC-1-PVA/PTFE membrane decreased from 73 to 51.9 kg m^{-2} h^{-1} over 24 h, while the permeate solution conductivity increased after 16 h. The deteriorating desalination properties were due to the pinhole defects on the PVA layer (Fig. S5a†). At the beginning of the experiment, the pinholes in the PVA layer led to higher water fluxes than the defect-free SC-2.6-PVA/PTFE membrane. However, NaCl and Tween 20 were transported with liquid water through the pinholes. As water was vaporized, NaCl crystallised and Tween 20 accumulated at the surface of the PTFE porous substrate. As a result, the salt scale and organic fouling blocked the pores of the PTFE substrate, causing water flux of the SC-1-PVA/PTFE membrane to decrease over time. Without these defects, the water flux of SC-2.6-PVA/PTFE membranes remained stable at 64.6 ± 2.6 kg m^{-2} h^{-1} over 24 h, demonstrating a better resistance against organic fouling.

Other than desalinating water/salt mixtures that are identical to seawater, we also characterised the desalination performances of the PTFE and SC-2.6-PVA/PTFE membranes using concentrated brine solutions where the NaCl content was between 5 and 25 wt%. As salt concentrations increased from 5 to 25 wt%, the water fluxes of the PTFE membrane decreased from 70.3 ± 0.6 to 25.9 ± 0.5 kg m^{-2} h^{-1} in DCMD mode; while those of the SC-2.6-PVA/PTFE membrane reduced from 60.5 ± 3.7 to 22.4 ± 4.3 kg m^{-2} h^{-1} in DCMD mode and 141.7 ± 0.1 to 30.5 ± 5.9 kg m^{-2} h^{-1} in PV mode (Fig. 5e). The conductivity of the PTFE membrane permeate side solution increased with a higher salt content (Fig. 5f). This was due to the formation of salt crystals on the PTFE membrane surface *i.e.* ionic fouling, which hydrophilized the membrane surface, leading to partial wetting of the PTFE pores.[45] Meanwhile in SC-2.6-PVA/PTFE

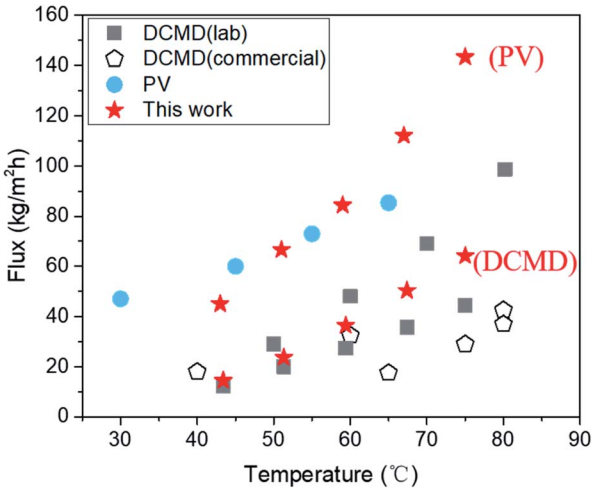

Fig. 6 Comparing desalination performances of the SC-2.6-PVA/PTFE membrane in both DCMD and PV modes with those of other PV desalination and DCMD membranes using a water solution containing 3.5 wt% NaCl as feed at temperatures from 20 to 90 °C.

composite membranes, the dense PVA layer prevented contact between salt crystals and the surface of PTFE fibrous supports. Therefore, the PTFE layer was able to maintain hydrophobicity and a high salt rejection rate. However, the water fluxes of SC-2.6-PVA/PTFE composite membranes decreased faster with a higher salt content in PV mode, possibly due to severe concentration polarisation effects on the feed side.[46]

Despite these impediments, SC-2.6-PVA/PTFE composite membranes continue to demonstrate high-water fluxes of 120.6 ± 4.2 kg m^{-2} h^{-1} in PV mode and 56.6 kg m^{-2} h^{-1} in DCMD mode for 10 wt% NaCl aqueous solution, highlighting the potential of such composites for recovering a concentrated brine solution. Meanwhile, the water fluxes of our membranes in DCMD mode were higher than those of commercially available DCMD membranes and on par with the best DCMD membranes prepared in labs[23,40,47,48] (Fig. 6). Clearly, regardless of desalination modes, the ability to overcome the incompatibility between PVA and PTFE *via* spray coating is key for salt/water separation performance that surpasses those of commercial and state-of-the-art membranes.

Conclusions

We demonstrated that the incompatibility between a hydrophilic polymer, PVA, and a hydrophobic PTFE porous support can be overcome with a simple and robust technique, spray coating. The strong adhesion between spray coated PVA and PTFE supports avoided the need to use an intermediate polymer layer to overcome the significant difference in the surface energy between these incompatible materials. As a result, the water flux of the spray coated PVA/PTFE membrane in DCMD mode reached 64.2 ± 2.9 kg m^{-2} h^{-1} with a high salt rejection over 99.9% at a feed temperature of 75.0 ± 0.9 °C. This separation performance is competitive with that of the best commercial DCMD membranes. In addition, spray coated composite membranes were more resistant to both organic and ionic fouling during long-term desalination experiments. In PV mode, the PVA/PTFE composite membranes demonstrated a water flux of 143.4 ± 8.9 kg m^{-2} h^{-1} at 75 °C, outperforming existing PV desalination membranes. The excellent desalination performance of spray coated PVA/PTFE composites was upheld even with brine solutions. In summary, we have demonstrated a facile method to fabricate high performance polymer composites that may transform the way desalination is achieved.

Conflicts of interest

There are no conflicts of interest to declare.

Acknowledgements

This research was funded by the National Natural Science Foundation of China (51773011). CHL acknowledges the financial support from the Chancellor's Fellowship of The University of Edinburgh.

References

1 D. S. Sholl and R. P. Lively, *Nature*, 2016, **532**, 435–437.
2 E. Jones, M. Qadir, M. T. H. Van Vliet, V. Smakhtin, V. Smakhtin and S.-M. Kang, *Sci. Total Environ.*, 2019, **657**, 1343–1356.
3 K. Scott, *Handbook of Industrial Membranes*, 2nd edn, 1998.
4 J. Mansouri, S. Harrisson and V. Chen, *J. Mater. Chem.*, 2010, **20**, 4567.
5 E. Guillen-Burrieza, A. Ruiz-Aguirre, G. Zaragoza and H. A. Arafat, *J. Membr. Sci.*, 2014, **468**, 360–372.
6 J. L. Xu, N. M. Srivatsa Bettahalli, S. Chisca, M. K. Khalid, N. Ghaffour, R. Vilagines and S. P. Nunes, *Desalination*, 2018, **432**, 32–39.
7 P. Peng, A. G. Fane and X. D. Li, *Desalination*, 2005, **173**, 45–54.
8 P.-J. Lin, M.-C. Yang, Y.-L. Li and J.-H. Chen, *J. Membr. Sci.*, 2015, **475**, 511–520.
9 L. Madauss, J. Schumacher, M. Ghosh, O. Ochedowski, J. Meyer, H. Lebius, B. Ban-d'Etat, M. E. Toimil-Molares, C. Trautmann, R. G. H. Lammertink, M. Ulbricht and M. Schleberger, *Nanoscale*, 2017, **9**, 10487–10493.
10 H. Chen, L. Bednarova, R. Besser and W. Lee, *Appl. Catal., A*, 2005, **286**, 186–195.
11 A. Simaite, B. Tondu, P. Soueres and C. Bergaud, *ACS Appl. Mater. Interfaces*, 2015, **7**, 19966–19977.
12 A. Baldan, *J. Mater. Sci.*, 2004, **39**, 1–49.
13 L. Chen, Z. D. Gu, L. Li, W. W. Lei, Q. F. Rong, C. Q. Zhao, Q. S. Wu, Z. Gu, X. Jin, L. Jiang and M. Liu, *J. Mater. Chem. A*, 2018, **6**, 15147–15153.
14 J. Q. Wang, C. C. Li, F. Wang, B. Yu, Y. Y. Luo, H. Z. Zeng and H. L. Zhu, *Prog. Org. Coat.*, 2019, **135**, 565–573.
15 H. M. Song, H. W. Yu, L. J. Zhu, L. X. Xue, D. C. Wu and H. Chen, *React. Funct. Polym.*, 2017, **114**, 110–117.

16 A. G. Lin, S. Shao, H. Z. Li, D. Y. Yang and Y. Kong, *J. Membr. Sci.*, 2011, **371**, 286–292.
17 E. Adem, M. Avalos-Borja, E. Bucio, G. Burillo, F. F. Castillon and L. Cota, *Nucl. Instrum. Methods Phys. Res., Sect. B*, 2005, **234**, 471–476.
18 C.-Y. Tu, Y.-C. Wang, C.-L. Li, K.-R. Lee, J. Huang and J.-Y. Lai, *Eur. Polym. J.*, 2005, **41**, 2343–2353.
19 X. Wang, Y. X. Tian, Z. B. Wang and Y. Tao, *J. Macromol. Sci., Part B: Phys.*, 2010, **50**, 172–178.
20 Q.-C. Xia, M.-L. Liu, X.-L. Cao, Y. Wang, W. H. Xing and S.-P. Sun, *J. Membr. Sci.*, 2018, **562**, 85–111.
21 D. Bhandari, K. O. Olanrewaju, N. Bessho, V. Breedveld and W. J. Koros, *Sep. Purif. Technol.*, 2013, **104**, 68–80.
22 D. J. Gardner, M. Blumentritt, L. Wang and N. Yildirim, *Rev. Adhes. Adhes.*, 2014, **2**, 127–172.
23 J. Q. Meng, P. Li and B. Cao, *ACS Appl. Mater. Interfaces*, 2019, **11**, 28461–28468.
24 B. Liang, Q. Li, B. Cao and P. Li, *Desalination*, 2018, **433**, 132–140.
25 Y. L. Xue, C. H. Lau, B. Cao and P. Li, *J. Membr. Sci.*, 2019, **575**, 135–146.
26 Y. L. Xue, J. Huang, C. H. Lau, B. Cao and P. Li, *Nat. Commun.*, 2020, **11**, 1461.
27 R. Takata, T. Iwao and M. Yumoto, *Electronics and Communications in Japan*, 2016, **99**, 93–99.
28 S. S. Feng, Z. X. Zhong, Y. Wang, W. H. Xing and E. Drioli, *J. Membr. Sci.*, 2018, **549**, 332–349.
29 S. K. Xue, C. C. Li, J. M. Li, H. L. Zhu and Y. H. Guo, *J. Membr. Sci.*, 2017, **524**, 409–418.
30 F. Wang, H. L. Zhu, H. P. Zhang, H. Y. Tang, J. Y. Chen and Y. H. Guo, *Journal of Water Process Engineering*, 2015, **8**, 11–18.
31 L. Setiawan, L. Shi, W. B. Krantz and R. Wang, *J. Membr. Sci.*, 2012, **423–424**, 73–84.
32 X.-M. Li, Y. Ji, Y. Yin, Y.-Y. Zhang, Y. Wang and T. He, *J. Membr. Sci.*, 2010, **352**, 173–179.
33 D. F. Li, T.-S. Chung and R. Wang, *J. Membr. Sci.*, 2004, **243**, 155–175.
34 X. Deng, F. Schellenberger, P. Papadopoulos, D. Vollmer and H.-J. Butt, *Langmuir*, 2013, **29**, 7847–7856.
35 L. Li, J. W. Hou, Y. Ye, J. Mansouri and V. Chen, *Desalination*, 2017, **422**, 49–58.
36 Z. L. Xie, M. Hoang, T. Duong, D. Ng, B. Dao and S. Gray, *J. Membr. Sci.*, 2011, **383**, 96–103.
37 I. Prihatiningtyas, A. Volodin and B. Van der Bruggen, *Ind. Eng. Chem. Res.*, 2019, **58**, 14340–14349.
38 C. Zhou, J. J. Zhou and A. S. Huang, *Microporous Mesoporous Mater.*, 2016, **234**, 377–383.
39 R. Zhang, B. Liang, T. Qu, B. Cao and P. Li, *Environ. Technol.*, 2019, **40**, 312–320.
40 G. Z. Liu, J. Shen, Q. Liu, G. P. Liu, J. Xiong, J. Yang and W. Q. Jin, *J. Membr. Sci.*, 2018, **548**, 548–558.
41 A. Trentin, C. Güell, T. Gelaw, S. de Lamo and M. Ferrando, *Sep. Purif. Technol.*, 2012, **88**, 70–78.
42 H. J. Tanudjaja and J. W. Chew, *J. Membr. Sci.*, 2018, **560**, 21–29.
43 H. Rabiee, S. M. S. Shahabadi, A. Mokhtare, H. Rabiei and N. Alvandifar, *J. Environ. Chem. Eng.*, 2016, **4**, 4050–4061.
44 L. Han, Y. Z. Tan, C. Xu, T. Xiao, T. A. Trinh and J. W. Chew, *J. Membr. Sci.*, 2019, **588**, 117196.
45 M. Rezaei, D. M. Warsinger, V. J. Lienhard, M. C. Duke, T. Matsuura and W. M. Samhaber, *Water Res.*, 2018, **139**, 329–352.
46 Q. Z. Wang, N. Li, B. Bolto, M. Hoang and Z. Xie, *Desalination*, 2016, **387**, 46–60.
47 P. Wang, M. M. Teoh and T.-S. Chung, *Water Res.*, 2011, **45**, 5489–5500.
48 M. M. A. Shirazi, A. Kargari and M. Tabatabaei, *Chem. Eng. Process.*, 2014, **76**, 16–25.